GRAPHENE AND 2DM VIRTUAL CONFERENCE & EXPO

Graphene online 2020 October 19-23

Edge State Crossing in a Multi-Band Tight-Binding Model of Graphene

Thorben Schmirander, Daniela Pfannkuche and Marta Prada

MOTIVATION

- Graphene nanoribbons terminated by zigzag edges: **Topological insulators**
- Intrinsic spin-orbit coupling: **Conducting helical edge states** at sample boundaries cross the Brillouin zone between Dirac points [1,2]
- **Multi-orbital tight-binding model** with p_z-, d_{xz}- and d_{yz}-orbitals
- Coulomb interactions change dispersion of edge states, treated in tight-binding model via **effective mean-field**
- **Three different magnetic phases** of edge states with different topological properties
- **ground state of nanoribbons** with different sizes, energies of edge magnetic phases for **different interaction strengths**
- Coulomb interactions in **higher-energy d-orbitals** is analyzed and **compared to single-orbital model**

MULTI-BAND TIGHT-BINDING MODEL OF GRAPHENE

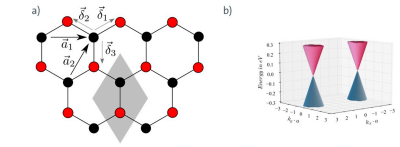

Fig. 1: a) The honeycomb lattice of graphene with lattices A and B. The lattice vectors are $\vec{a}_1$ and $\vec{a}_2$, the vectors $\vec{\delta}_1$, $\vec{\delta}_2$ and $\vec{\delta}_3$ point to the nearest neighbors. The primitive unit cell is shaded gray. **b)** The two non-equivalent Dirac cones in graphene.

- Effective **low-energy Hamiltonian** with the sublattice spin $\hat{\sigma}$ and the valley isospin $\hat{\tau}_z$ (Fig. 1a + 1b)

$$H_0 = -v_F \hbar(\hat{\tau}_z \hat{\sigma}_x k_x + \hat{\sigma}_y k_y)$$

- Multi-orbital tight-binding model is defined via

$$H_{\mathbf{k}} = \sum_{\mu\nu} E_\mu \delta_{\mu\nu} (\hat{\alpha}^{\mu\dagger}_{\mathbf{k}} \hat{\alpha}^{\nu}_{\mathbf{k}} + \hat{\beta}^{\mu\dagger}_{\mathbf{k}} \hat{\beta}^{\nu}_{\mathbf{k}}) + \sum_{\mu\nu} \sum_{i=1}^{3} e^{-i\vec{\delta}_i \mathbf{k}} t^{\mu\nu}(\vec{\delta}_i/a) \hat{\alpha}^{\mu\dagger}_{\mathbf{k}} \hat{\beta}^{\nu}_{\mathbf{k}} + \text{h.c.}$$

- Included: Real spin + orbitals $\mu, \nu \in \{p_z, d_{xz}, d_{yz}\}$
- ladder operators for the A and B sublattices $\hat{\alpha}_{\mathbf{k}}$ and $\hat{\beta}_{\mathbf{k}}$
- Periodic in one direction and terminated by **zigzag edges** in the other (Fig. 2a)
- Edge states: **peak** in **density of states** (Fig. 2b)
- dispersion of edge states in the single-orbital model is flat (Fig 2c, left)
- d-orbitals break electron-hole symmetry (Fig 2c, right)
- **Slater-Koster approximation** is used for hopping matrix elements (Fig. 2d)

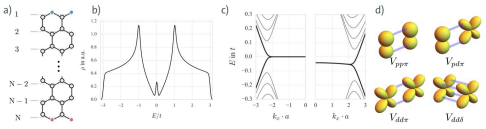

Fig. 2: a) The unit cell is comprised of N rows and 4 columns is terminated by zigzag edges. Two edge states at $k_x = 0$ are depicted in red and blue. **b)** The edge states result in a pronounced peak in the density of states. **c)** The dispersion relation of the edge states (bold) of the single-orbital model (left) and of the multi-orbital tight binding model (right). **d)** The different material parameters used in the Slater-Koster approximation [3].

ELECTRONIC INTERACTIONS IN A MULTI-ORBITAL TIGHT-BINDING MODEL

- Matrix elements p_z-orbitals: by index p and those for the d-orbitals by index $n \in \{1, \ldots, 5\}$
- **On-site interaction** Hamiltonian in multi-orbital tight-binding model:

$$H^{ee}_{pd} = U_p \hat{n}_{p\uparrow} \hat{n}_{p\downarrow} + \sum_n \Big(V_n \left(\hat{n}_{p\uparrow}\hat{n}_{n\downarrow} + \hat{n}_{p\downarrow}\hat{n}_{n\uparrow}\right) + J_n \left(\hat{c}^\dagger_{p\uparrow}\hat{c}^\dagger_{n\downarrow}\hat{c}_{p\downarrow}\hat{c}_{n\uparrow} + \hat{c}^\dagger_{p\downarrow}\hat{c}^\dagger_{n\uparrow}\hat{c}_{p\uparrow}\hat{c}_{n\downarrow}\right) + (V_n - J_n)\left(\hat{n}_{p\uparrow}\hat{n}_{n\uparrow} + \hat{n}_{p\downarrow}\hat{n}_{n\downarrow}\right)\Big).$$

- First term: **Single-orbital Hubbard term** for p_z-orbitals with interaction U
- Second: Coulomb repulsion of electrons in **different orbitals**, with **different spins**
- Third: Non-classical **exchange**
- Forth: Coulomb repulsion of electrons in **different orbitals** with **same spin**
- interaction matrix elements for d-orbitals are considered the same: $V := V_n$ and $J := J_n$
- **only two d-orbitals** couple to p-orbitals by symmetry (n=2)
- **mean-field approximation**:

$$\hat{n}_\uparrow \hat{n}_\downarrow = (\langle\hat{n}_\uparrow\rangle + \Delta\hat{n}_\uparrow)(\langle\hat{n}_\downarrow\rangle + \Delta\hat{n}_\downarrow) \approx -\langle\hat{n}_\uparrow\rangle\langle\hat{n}_\downarrow\rangle + \hat{n}_\uparrow\langle\hat{n}_\downarrow\rangle + \hat{n}_\downarrow\langle\hat{n}_\uparrow\rangle$$

THE HARTREE-FOCK METHOD AND BREAKING SYMMETRIES

- Hartree-Fock method approximates **electronic interactions** via a **self-consistent field** [4]
- **different symmetries must be broken** in the initial matrix elements before the first computation, for reaching specific types of solutions
- ferromagnetic edge phase (**FM**): **time-reversal symmetry** (TR) must be broken, which is achieved by a half-filled system with a spin imbalance
- antiferromagnetic edge phase (**AFM**): **spin-spatial symmetry** must be broken, such that the edges exhibit opposing spin polarization with respect to each other at half-filling
- **non-magnetic** edge phase: **electron-hole symmetry** (EH) must be broken and a doped solution is computed. Possible by changing the chemical potential of the system with an offset from half-filling.

NON-MAGNETIC EDGE PHASE

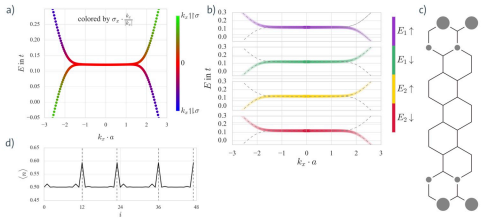

Fig. 3: a) Dispersion relation of the edge states in the non-magnetic edge phase. The model has 12x4 sites and only a single-band. **b)** The four individual energy bands colored by sublattice spin and real spin expectation values. **c)** The occupation of two edge states located at opposing edges. Occupation has contributions from both spin up and down in equal amounts. **d)** Particle number expectation value per site. The four sites of the edges are marked by dashed vertical lines.

- **Non-magnetic edge phase similar to non-interacting system** (Fig. 3a, 2c)
- Four states **cross band gap** according to their edge helicity: **alignment of sublattice and real spin** (Fig. 3b)
- **Density accumulates** at only one sublattice at each edge (Fig. 3c, 3d)
- can only be **obtained with doping**: **changes energy** of the phase compared to half-filling
- Energy difference between a solution at doping obtained with self-consistency and at half filling (Fig. 4a, 4b)

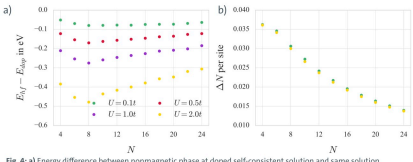

Fig. 4: a) Energy difference between nonmagnetic phase at doped self-consistent solution and same solution computed at half-filling for ribbons of size Nx4 sites. Single band-model for different U. **b)** Particle number difference of doped solution from half-filling as in a).

FERROMAGNETIC EDGE PHASE

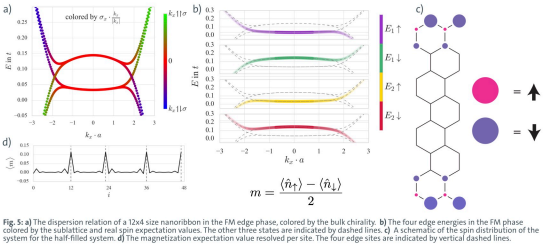

$$m = \frac{\langle\hat{n}_\uparrow\rangle - \langle\hat{n}_\downarrow\rangle}{2}$$

Fig. 5: a) The dispersion relation of a 12x4 size nanoribbon in the FM edge phase, colored by the bulk chirality. **b)** The four edge energies in the FM phase colored by the sublattice and real spin expectation values. The other three states are indicated by dashed lines. **c)** A schematic of the spin distribution of the system for the half-filled system. **d)** The magnetization expectation value resolved per site. The four edge sites are indicated by vertical dashed lines.

- FM phase: **Two spin-up states are lower in energy**, indicated by **energy gap** of the two states at each edge (Fig. 5a, 5b)
- **Occupy different sublattices** (Fig. 5c). Edge atoms exhibit parallel spin polarization on one sublattice, other sublattice is polarized in opposing direction: **local ferrimagnetic structure**
- Both **edges have parallel spin alignment** with respect to each other (Fig. 5d)

ANTI-FERROMAGNETIC EDGE PHASE

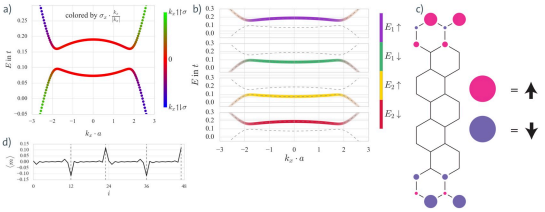

Fig. 6: a) Dispersion relation of 12x4 size nanoribbon in AFM edge phase **b)** Four edge state energies of the AFM phase colored by sublattice and real spin expectation values. Other states are indicated by dashed lines. **c)** Schematic of spin types occupying each site of the nanoribbon at half-filling. **d)** The magnetization expectation value resolved per site. The four edge sites are indicated by vertical dashed lines.

- AFM phase: **Band structure exhibits a gap** (Fig. 6a)
- Two states with **anti-parallel sublattice and real spin** are **lower in energy** compared to parallel alignment (Fig. 6b)
- At each edge: **local ferrimagnetic structure**
- both e**dges have anti-parallel spin alignment** (Fig. 6c, 6c)

PHASE TRANSITIONS IN A SINGLE-ORBITAL MODEL

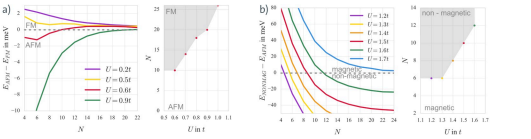

Fig. 7: a) Energy differences between the two magnetic phases for nanoribbons of different sizes for different U (left). The points of transition from an AFM to FM phase for different ribbon lengths N and interaction strengths U (right). **b)** The energy difference between the non-magnetic and AFM phase at different ribbon sizes for different U (left). The point of phase transition from a non-magnetic ground state to a magnetic ground state for ribbons of different sizes and interaction strenghts (right).

- Energy difference of magnetic phases for nanoribbons of different sizes and U (Fig. 7 a, left)
- Transition point: **FM phase** is preferred for **weak interactions and long ribbons** (Fig. 7 a, right)
- **AFM** edge phase: **very short ribbons and strong interactions**
- **Non-magnetic** ground state: **weak interactions** (Fig. 7 b, left and right)

SIZE-DEPENDENCE OF MAGNETIC PHASES

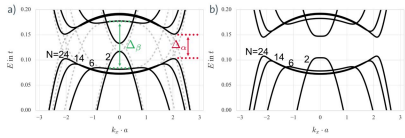

Fig. 8: a) The dispersion relations of the FM edge phase for nanoribbons of different sizes, as indicated by the numbers. The energy difference of the states at the Γ- point is defined as Δ_α and at the minimum of the non-crossing states as Δ_β. In the FM phase this is no true gap, but defined for comparison. The dashed lines indicate these states crossing the band gap. **b)** The dispersion relation of the AFM phase for nanoribbons of different sizes, as indicated by the numbers.

- **Dispersion relation** of the FM phase (Fig. 8 a), and AFM phase (Fig. 8 b) **change with number of rows** N
- **Two types of gaps**: can be **related to Coulomb interaction** strength (Fig. 9)

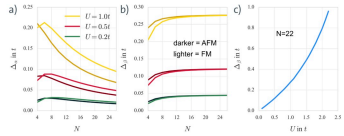

Fig. 9: a) The gap Δ_α as defined in Fig. 8, for different interaction strengths and different ribbon lengths. **b)** The gap Δ_β for different ribbon sizes. The lighter shade is the gap of the FM phase and the darker that of the AFM phase. **c)** At sufficiently large ribbons, such as N=22, the gap Δ_β depends only on the interaction parameter U.

- Gap Δ_α marks **band gap of AFM phase** and for non-crossing states in FM phase (Fig. 9 a) for comparison
- **Increases with U**, larger for FM phase with nearly constant offset from AFM phase
- **Decreases for longer nanoribbons**
- Gap Δ_β **converges to constant value** as length increases (Fig. 9 b), only depends on U (Fig. 9 c)

PHASE TRANSITIONS IN A MULTI-ORBITAL MODEL

INFLUENCE OF D-ORBITALS

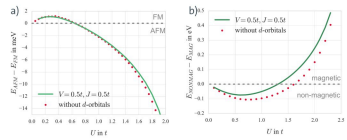

Fig. 11: a) The energy difference between the AFM and FM phase with and without d-orbitals for N=12 and different U. **b)** Energy differences between the non-magnetic and the lower-energy magnetic phase for the single-orbital and multi-orbital model for N=12.

- **Inclusion of d-orbitals** in multi-band tight-binding model changes dispersion relation of edge states and energy of the phases
- Low DOS at Fermi level: **magnetic phases are nearly unaffected** (Fig. 11a)
- Peak in DOS (Fig. 2b): **Energy of non-magnetic phase changes due to d-orbitals** (Fig. 11b)

INTERACTIONS IN D-ORBITALS

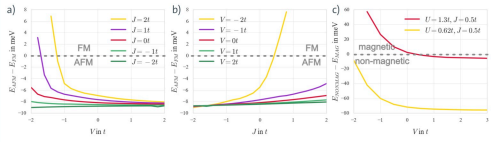

Fig. 12: a) The energy difference between the two magnetic edge phases in dependence of V for different J and U=1.6t and N=12. **b)** The energy difference between the two magnetic edge phases in dependence of J for different V and U=1.6t and N=12. **c)** Energy difference between the non-magnetic and the lower-energy magnetic phase in dependence of V for two different U and N=12.

- @U = 1.6t: **Ground state is the AFM phase** (Fig. 11a, 11b)
- Large **attractive V**: Ground state can be **FM phase** (Fig. 12a, 12b)
- Attractive V: **Change non-magnetic ground state** @ U=1.3t **to magnetic** (Fig. 12c)

SUMMARY

- Electronic **interactions implemented via mean-field** method in **multi-band tight-binding model**
- **three magnetic edge phases** identified and characterized
- **Non-magnetic phase is topological insulator**, exists in the case of **doping**, features **density at zigzag edges** and is **ground state for weak Coulomb interaction** strengths
- **increased U**: **Ground state becomes topologically trivial AFM** edge phase
- **Including d-orbitals**: **Energy of non-magnetic phase is increased** due to large DOS at the Fermi energy
- **large attractive V** : Affect ground state of the system, because **occupation of d-orbitals is increased**
- Then: **Magnetic ground state** at U = 1.6t **may become FM**, difference to single-orbital model.
- **Energy of non-magnetic edge phase influenced by attractive interaction**: At smaller U edge magnetic phase may become ground state

CONTACT PERSON

Thorben Schmirander

I. Institute for Theoretical Physics
University of Hamburg, Germany
Jungiusstraße 9, 20355 Hamburg

Thorben.schmirander@physik.uni-hamburg.de

REFERENCES

[1]: Castro Neto et. al. Rev. Mod. Phys. **81**, 109 (2009)
[2]: Kane and Mele, Phys. Rev. Lett. **95**, 146802 (2005)
[3]: Slater and Koster, Phys. Rev. **94**, 1498 (1954)
[4]: Claveau et. al. Eur. J. Phys. **35** 035023 (2014)

Graphene online 2020